INSTITUTE OF PLASMA PHYSICS

NAGOYA UNIVERSITY

Fokker-Planck Calculation of Hot Electron Formation in the Thermal Barrier Region of Tandem Mirror GAMMA 10

I. Katanuma, Y. Kiwamoto, K. Sawada, S. Miyoshi

(Received – Mar. 7, 1984)

IPPJ- 726 Apr. 1984

RESEARCH REPORT

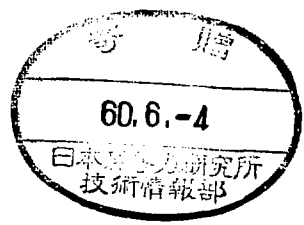

NAGOYA, JAPAN

Fokker-Planck Calculation of Hot Electron Formation in the Thermal Barrier Region of Tandem Mirror GAMMA 10

I. Katanuma*, Y. Kiwamoto*, K. Sawada*, S. Miyoshi*

(Received - Mar. 7, 1984)

IPPJ - 726 Apr. 1984

Further comunication about this report is to be sent to the Research Information Center, Institute of Plasma Physics, Nagoya University, Nagoya Japan.

---

* Plasma Research Center, the University of Tsukuba, Ibaraki 305 Japan.

Abstract

We have studied the hot electron build-up by the second harmonic electron cyclotron resonance heating in the thermal barrier region of tandem mirror GAMMA 10 by using a Fokker-Planck code with self-consistent potential profile taken into account. We have found two phases in the evolution of hot electron population and the potential profile. In the first phase where the RF diffusion is dominant quick increase of the hot electron density and that of the mean energy are observed. No further increase in the mean energy is observed thereafter. The potential is the deepest during the first phase. The second phase starts in the mean-free-time of the pitch angle scattering of hot electrons on cold electrons and ions. In this phase the hot electron population increases in the rate of the pitch angle scattering. The potential dip shallows due to the accumulation of pitch angle scattered passing ions. This observation indicates the necessity of the ion pumping for maintaining the negative potential at the thermal barrier.

1. Introduction

Tandem mirror GAMMA 10 employs thermal barrier to insulate the electrons in the end plugs from those in the central cell. Generation of thermal barrier requires the creation of a high population of mirror trapped hot electrons, heated by electron cyclotron resonance heating (ECRH). The idea of thermal barrier is introduced in favor that the plug potential can be formed even if the plug density n_p is lower than the central density n_c when there is a potential depression between the plug and the central cell[1),2)]. The reduced requirement on plug density to establish the plug potential significantly reduces the magnet and neutral beam technology constraints and the power requirements for end plugging of tandem mirrors.

Tandem mirror GAMMA 10 at Univ. Tsukuba employs ECRH to form the thermal barrier and plug potential in each end cell[3)]. Four 140kW 28GH$_z$ gyrotrons are used in the thermal barrier and end plug regions for electron heating. Resonant absorption of the extraordinary mode wave is expected at the second harmonic resonance in thermal barrier and at the fundamental resonance in the plug.

In this paper theoretical and numerical studies are made on the creation of hot electron population when only second harmonic electron cyclotron resonsnce heating is applied in the thermal barrier region. In Sec.2 we analytically evaluate the time scale of hot electron build up in the thermal barrier region. In Sec.3 we describe the numerical scheme of the bounce averaged Fokker-Planck code which is capable of calculating the self-consistent electrostatic potential. Section 4

shows the results of the simulation study of hot electron formation by means of the bounce averaged Fokker-Planck code. We clarify the mechanism of hot electron build up and point out the necessity of cold ion pumping. Summary of this paper is made in Sec.5.

2. Evaluation of Characteristic Time Scale

To control the thermal barrier potential, it is necessary to control hot electron population in the thermal barrier region. Electron cyclotron resonance heating of hot electrons in tandem mirror is an area of active experimental and theoretical investigations[4,5]. However the hot electron build up process has not been examined in the self-consistent electrostatic potential profile.

In order to produce a substantial amount of hot electron density within a limitation of beta value for MHD stability[3,6], the mean energy of hot electrons needs to be limited. The microwave power absorption by runaway electrons may be limited by means of detuning from the resonance frequency due to relativistic mass shift. This idea may be embodied by spatial localizing the microwave power in a region where the resonance condition $\omega = 2\omega_{ce}/\gamma$ is satisfied only for low energy electrons say with few tens of keV. Here ω is the wave frequency, ω_{ce} is electron cyclotron frequency, $\gamma = 1/(1-v^2/c^2)^{1/2}$, and v is the electron velocity, and c is light speed. In experimemt, a narrow pencil beam of microwave is injected in X-mode (R-wave)

possesing higher absorption efficiency.

Microwaves have sufficiently short wave length so that the propagating character can be predicted by ray tracing techinique. Furthermore microwaves are not as susceptible to nonlinear effects as some other wave heating methods, so spatial locations of wave can be predicted easily from linear theory[7]. To study the hot electron build up in thermal barrier region theoretically and numerically, we include the quasilinear electron heating effects[8] in Fokker-Planck equation.

$$\frac{\partial f}{\partial t} = (\frac{\partial f}{\partial t})_c + \frac{\partial}{v_\perp \partial v_\perp}(v_\perp D \frac{\partial f}{\partial v_\perp}), \tag{1}$$

$$D = \pi(\frac{e}{2m_e\omega})^2 \sum_l l^2\omega_{ce}^2 |E^+|^2 \delta(\omega - l\omega_{ce}/\gamma) J_{l-1}^2(\frac{k_\perp v_\perp}{\omega_{ce}}),$$

$$E^+ = E_x + iE_y,$$

Here we use standard notation and E^+ is the electric field of the right hand polarized microwave, $k_\perp$ is perpendicular mode number, J_{l-1} is Bessel function, $v_\perp$ is the perpendicular velocity component, and $\delta()$ is Dirac delta function. The first term in the right hand side of Eq.(1) is Fokker-Planck collision term. We assume $k_\parallel=0$ and $E_\parallel=0$ for simplicity.

At first by using Eq.(1), we evaluate the characteristic time of hot electron build up when only second harmonic resonance heating are applied at the midplane.

Bounce averaging Eq.(1) along particle orbits assuming $\gamma=1$, we

have

$$\frac{\partial f}{\partial t} = \frac{\partial}{v_\perp \partial v_\perp}(v_\perp \langle D \rangle \frac{\partial f}{\partial v_\perp}), \tag{2}$$

$$\langle D \rangle = \int_{orbit} D \frac{dz}{v_\parallel} \Big/ \int_{orbit} \frac{dz}{v_\parallel}$$

$$= 2\pi (\frac{e}{2m_e})^2 \frac{1}{\omega} |E^+|^2 J_1^2 \Big/ (\tau_B \frac{dB}{Bdz}),$$

$$\tau_B = v_\parallel \int_{orbit} \frac{dz}{v_\parallel}.$$

Here $v_\parallel$ and $v_\perp$ are the velocity components at the midplane of a mirror cell, z is the coordinate along magnetic field line, and we consider only ECRH term of Eq.(1). By integrating Eq.(2) multiplied with $(1/2)m_e v_\perp^2$, we have a equation for hot electron build up at the midplane as

$$\frac{\partial}{\partial t} n_h T_{h\perp} = \frac{n_h T_{h\perp}}{\tau_b}, \tag{3}$$

$$\tau_b^{-1} = 4\pi (\frac{e}{2m_e})^2 |E^+|^2 N_\perp^2 \Big/ (\omega \tau_B c^2 \frac{dB}{Bdz}),$$

$$N_\perp = k_\perp c/\omega.$$

For the thermal barrier region of GAMMA 10 we obtain τ_b numerically as,

$$\tau_b = 2.36\times10^{-6}\frac{\omega}{\omega_{c0}} \Big/ \{(\frac{|E^+|}{100})^2 N_\perp^2\} \qquad sec. \tag{4}$$

Here ω_{c0} is the electron cyclotron frequency for B = 10 kgauss, $|E^+|$ is measured by a unit of V/cm. For $|E^+|=100V/cm$, $N_\perp=1$, $\omega/\omega_{c0}=1$, we have $\tau_b\sim2.36\mu sec$. Roughly speeking, τ_b is the time in which runaway electron population is driven by ECRH power, i.e. RF diffusion time.

The RF diffusion time τ_b is so fast compared to electron collision time, as is shown later in this paper, that the quasi-steady state will be realized in which hot electron pitch angle scattering will contribute to the further evolution of hot electron density in the thermal barrier region.

Next we consider the effects of the hot electron pitch angle scattering. In this quasi-steady state, the following equation will hold as the first approximation,

$$\frac{\partial}{v_\perp \partial v_\perp}(v_\perp \langle D\rangle \frac{\partial f_h}{\partial v_\perp}) = 0, \tag{5}$$

on $v_\parallel=0$ line at the midplane of the mirror cell. Here f_h is the hot electron distribution function at the midplane. One of the solution of Eq.(5) is

$$f_h(v) = \frac{n_h}{2\pi v_{max}} v^{-2}\delta(\theta-\pi/2), \qquad v \leqq v_{max},$$

$$= 0, \qquad v > v_{max}. \tag{6}$$

Where n_h is the hot electron density, v_{max} is the maximum velocity of hot electrons, above which electrons are assumed not to be further heated by ECRH due to the relativistic electron mass shift. We use the spherical coordinate (v,θ,Φ). In order to take the collisional effects into account, we assume the electron distribution function as,

$$f(v,\theta) = \frac{n_c}{\pi^{3/2}v_e^3}exp(-\frac{v^2}{v_e^2}) + \frac{n_h}{2\pi v_{max}}v^{-2}\delta(\theta-\pi/2), \tag{7}$$

$$v_e^2 = 2T_e/m_e.$$

Here n_c, T_e are cold electron density and temperature, respectively. In this case linearized Fokker-Planck equation becomes

$$\frac{\partial f_h}{\partial t} = n_c\left[\frac{1}{v^2}\frac{\partial}{\partial v}(f_h+\frac{v_e^2}{2v}\frac{\partial f_h}{\partial v}) + \frac{1}{2v^3}\frac{\partial}{\partial \mu}\{(1-\mu^2)\frac{\partial f_h}{\partial \mu}\}\right]\Gamma$$

$$+ n_h\left[\frac{2}{v_{max}}v^{-2}\delta(\theta-\pi/2)f_h + \frac{1}{2v^2v_{max}}\ln\left|\frac{v+v_{max}}{v}\right|\frac{\partial^2 f_h}{\partial\theta^2}\right.$$

$$\left. + \frac{1}{2vv_{max}}(\ln\left|\frac{v+v_{max}}{v}\right| + \frac{v_{max}}{v})\frac{\partial f_h}{\partial v}\right]\Gamma. \tag{8}$$

Here $\Gamma=4\pi e^4\ln\Lambda/m_e^2$, $\mu=\cos\theta$ and $\ln\Lambda$ is Coulomb logarithm. Integrating Eq.(8) for (v,θ) assuming $\partial^2 f_h/\partial\theta^2 \sim -f_h/(\Delta\theta)^2$, and $\Delta\theta$ is the half width of the resonance region in electron velocity space at the midplane of mirror cell, we have

$$\frac{\partial n_h}{\partial t} = -(\frac{1}{\tau_{cd}} + \frac{1}{\tau_{cs}} + \frac{1}{\tau_{hd}} + \frac{1}{\tau_{hs}})n_h. \tag{9}$$

Here

$$\tau_{hs} = 4\tau_D \frac{n_c}{n_h} (\Delta\theta)^2 (\frac{E_{max}}{T_e}) (\frac{E_{min}}{T_e})^{1/2} / \ln(\frac{E_{max}}{E_{min}}),$$

$$\tau_{cs} = 4\tau_D (\Delta\theta)^2 (\frac{E_{max}}{T_e})^{1/2} (\frac{E_{min}}{T_e}),$$

$$\tau_{hd} = 2\tau_D \frac{n_c}{n_h} (\frac{E_{max}}{T_e})^{1/2} (\frac{E_{min}}{T_e}),$$

$$\tau_{cd} = \tau_D (\frac{E_{max}}{T_e})^{1/2} (\frac{E_{min}}{T_e}),$$

$$\tau_D = \frac{\sqrt{m_e/2}\, T_e^{3/2}}{\pi n_c e^4 \ln\Lambda}, \qquad E_{max} = \frac{1}{2} m_e v_{max}^2, \qquad E_{min} = \frac{1}{2} m_e v_{min}^2,$$

$$n_h = \int_{v_{min}}^{v_{max}} 2\pi v^2 dv \int_{\pi/2-\Delta\theta}^{\pi/2} \sin\theta d\theta f_h.$$

Here τ_{hs} is the escaping time of hot electrons out of the resonance region in the velocity space by hot-hot electron pitch angle scattering, τ_{cs} is that by hot-cold electron pitch angle scattering, τ_{hd} is that by hot-hot electron drag, τ_{cd} is that by hot-cold electron drag, and $\Delta\theta$ is measured in radian. Pitch angle scattering represents the hot electron drain from the RF diffusion zone in velocity space, contributing to activate the RF pump-up of the hot electron density from the cold region. Electron drag reduces the hot electron density.

For the parameters of n_c=10^{12}/cc , n_h=5×10^{11}/cc, T_e=100eV,

E_{max}=50keV , E_{min}=2keV , $\Delta\theta$=12° , we have τ_{hs}~4.2msec, τ_{hd}~31msec, τ_{cs}~1.4msec, τ_{cd}~7.8msec. The coulomb collision on ions contributes to pitch angle scattering of hot electrons on the same order as τ_{cs}. Therefore, the pitch angle scattering on cold electrons and ions is the dominant process controlling the hot electron density build up in the time scale of the order of 1 msec.

3. Fokker-Planck Code

To study plasma confinement in a mirror we use the Fokker-Planck equation. The loss rate is included in terms of coulomb collisions into the loss cone region in the velocity space. The loss cone is defined as the region where particles are not confined by either the axial magnetic field or the electrostatic potential. We assume the mean free path of particles is so long that the particle does not change its velocity so much during the bouncing period from one end of a mirror to the other. Then we can integrate the Boltzmann equation along a particle orbit in order to study the spatially varying distribution in mirror systems [9].

$$\frac{\partial}{\partial t} f(v_b, \theta_b) = \int_{orbit} \frac{dz}{v_\parallel} \left\{ \left(\frac{\partial f}{\partial t}\right)_c + D_h f \right\} \Big/ \int_{orbit} \frac{dz}{v_\parallel} . \qquad (10)$$

Here $f(v_b, \theta_b)$ is the distribution function at the midplane of a mirror cell, that is $f(v_b, \theta_b) = f(v, \theta, z=0)$. Gyromotion effects are

also integrated out. We neglect radial dependence assuming radial transport processes are slow compared to the axial one. $(\partial f/\partial t)_c$, is the local Fokker-Planck collision term, and the term of $D_h f$ represents ECRH heating which is the same as second term in right hand side of Eq.(1). To derive Eq.(10) the conservation of particle energy and magnetic moment are called for during the one particle bounce period along magnetic field.

We adopt the collision operator as follows,

$$(\frac{\partial f_t}{\partial t})_c = \sum_\alpha \{ - \frac{\partial}{\partial v_i}(f_t \frac{\partial h_\alpha}{\partial v_i}) + \frac{1}{2}\frac{\partial^2}{\partial v_i \partial v_i}(f_t \frac{\partial^2 g_\alpha}{\partial v_i \partial v_j})\}\Gamma_\alpha, \tag{11}$$

$$g_\alpha(\tilde{v}) = \int d\tilde{v}' f_\alpha(\tilde{v}') |\tilde{v}-\tilde{v}'|, \tag{12}$$

$$h_\alpha(\tilde{v}) = \frac{m_t+m_\alpha}{m_\alpha}\int d\tilde{v}' \frac{f_\alpha(\tilde{v}')}{|\tilde{v}-\tilde{v}'|}, \tag{13}$$

$$\Gamma_\alpha = \frac{4\pi q_\alpha^2 q_t^2}{m_t^2} \ln\Lambda_{\alpha t}.$$

Here v_i and v_j are the component of velocity, m_α is mass, n_α is number density, q_α is charge of α species, and subscript t stands for the particles of t species. $\ln\Lambda_{\alpha t}$ is coulomb logarithm. Equation (11) can be written as

$$(\frac{\partial f_t}{\partial t})_c = \sum_\alpha \{A_\alpha \frac{\partial^2 f_t}{\partial v_b^2} + B_\alpha \frac{\partial^2 f_t}{\partial v_b \partial \theta_b} + C_\alpha \frac{\partial^2 f_t}{\partial \theta_b^2} + D_\alpha \frac{\partial f_t}{\partial v_b} + E_\alpha \frac{\partial f_t}{\partial \theta_b} + F_\alpha f_t\}. \tag{14}$$

Here f_t, v_b, and θ_b are the quantities at the midplane of a mirror

cell. Since the contributions of the axial distribution of parameters are included only in the coefficients of Eq.(14), only these coefficients are to be bounce-averaged numerically. There are several methods to solve Eqs.(12) and (13) [10,11] . The distribution function can be expanded in Legendre polynomials.

$$f(\upsilon,\theta) = \sum_{k=0}^{\infty}\alpha_k(\upsilon)P_k(\cos\theta), \tag{15}$$

$$\alpha_k(\upsilon) = \int_{-1}^{1}d\cos\theta\ fP_k(\cos\theta) \ / \ \int_{-1}^{1}d\cos\theta\ P_k^2(\cos\theta).$$

Therefore Eqs.(12), (13) becomes

$$g_\alpha(\upsilon,\theta) = \sum_{k=0}^{\infty}\frac{4\pi}{2k+1}\upsilon^4P_k(\cos\theta)\{\frac{1}{2k+3}\{\frac{1}{\upsilon^{5+k}}\int_0^{\upsilon}\alpha_k(\upsilon')\upsilon'^{4+k}d\upsilon'$$

$$+ \frac{1}{\upsilon^{2-k}}\int_{\upsilon}^{\infty}\alpha_k(\upsilon')\upsilon'^{1-k}d\upsilon'\} - \frac{1}{2k-1}\{\frac{1}{\upsilon^{3+k}}\int_0^{\upsilon}\alpha_k(\upsilon')\upsilon'^{2+k}d\upsilon'$$

$$+ \frac{1}{\upsilon^{4-k}}\int_{\upsilon}^{\infty}\alpha_k(\upsilon')\upsilon'^{3-k}d\upsilon'\}\}, \tag{16}$$

$$h_\alpha(\upsilon,\theta) = \sum_{k=0}^{\infty}\frac{4\pi}{2k+1}\upsilon^2P_k(\cos\theta)\{\frac{1}{\upsilon^{2-k}}\int_{\upsilon}^{\infty}\alpha_k(\upsilon')\upsilon'^{1-k}d\upsilon'$$

$$+ \frac{1}{\upsilon^{3+k}}\int_0^{\upsilon}\alpha_k(\upsilon')\upsilon'^{2+k}d\upsilon'\}. \tag{17}$$

Here g_α and h_α are calculated numerically with the integration on υ' in Eqs.(16), (17). $\partial^2 g_\alpha/\partial\upsilon^2$, $\partial h_\alpha/\partial\upsilon$ are also written in the same

way as Eqs.(16), (17). Therefore Eq.(10) is written as a second partial differential equation, which is solved numerically by ADI method[10,11].

We take the boundary condition at the midplane as

$$\frac{\partial}{\partial\theta}f(v=0,\theta) = 0,$$

$$\frac{\partial}{\partial v}f(v=0,\theta=\pi/2) = 0, \tag{18}$$

$$\frac{\partial}{\partial\theta}f(v,\theta=0) = \frac{\partial}{\partial\theta}f(v,\theta=\pi/2) = 0.$$

where we assume the symmetry about $\theta=\pi/2$, and calculate nonlinear Fokker-Planck equation in the region $0\leqq v<\infty$ and $0\leqq\theta\leqq\pi/2$.

In integrating the equation $F=\int \tilde{v}^n f(\tilde{r},t)d\tilde{v}$ off the midplane a special care is in order. If we use the equation,

$$F = \int d\tilde{u}_b \frac{\partial(\tilde{v})}{\partial(\tilde{u}_b)} \{\tilde{u}_b^2 - \frac{2q}{m}(\varphi-\varphi_b)\}^{n/2} f(\tilde{u}_b), \tag{19}$$

where,

$$\frac{\partial(\tilde{v})}{\partial(\tilde{u}_b)} = \cos\theta_b / \sqrt{\psi(\cos^2\theta_b - 1 + \psi v^2/u_b^2)},$$

$$\psi = B_b/B,$$

we have a singular point coming from the Jacobian $\partial(\tilde{v})/\partial(\tilde{u}_b)$. Here B_b and φ_b are the magnetic field and the electrostatic potential at

the midplane, respectively. Instead we employ the moving velocity meshes along particle orbits. Numerically the distribution function $f(v_b,\theta_b)$ is determined for the each velocity mesh point at the midplane. The distribution function off the midplane connects with that at the midplane by the Liouville's theorem,

$$f(v,\theta,z) = f(v_b,\theta_b). \tag{20}$$

New mesh points off the midplane are given by the orbit equations representing the energy conservation and magnetic moment invariance as,

$$v^2 = v_b^2 + \frac{2q}{m}\varphi_b - \frac{2q}{m}\varphi(z), \tag{21}$$

$$v^2 \sin^2\theta = \frac{B(z)}{B_b} v_b^2 \sin^2\theta_b.$$

Then, by using the new moving velocity meshes off the midplane, we can easily obtain the integration F by numerical calculation without any singularity.

In calculating the density profile for the potential determination, a new coordinate (v_i,θ_i) is introduced which represents the mirror loss cone boundary in addition to the (v_i,θ_j) meshes on the velocity space. Here subscripts i, j are mesh numbers in the v and θ directions, respectively. The distribution function at the boundary (v_i,θ_i) is obtained by interpolation from the mesh points around it. The density of the mirror-trapped particles is determined by numerical

integration of the distribution function outside the loss cone.

Passing particle density and Yushimanov trapped particle density are calculated from analytic expression as follows. Let us consider the typical profile of the electrostatic potential in a single mirror cell as shown in Fig.1(a). In this system the ion and electron distribution function at the mirror throat are assumed as,

$$f_i = n_m \left(\frac{m_i}{2\pi T_i}\right)^{3/2} \exp\left(\frac{\varepsilon_i - q_i\varphi_0}{T_i}\right),$$

$$f_e = n_m \left(\frac{m_e}{2\pi T_e}\right)^{3/2} \exp\left(\frac{\varepsilon_e - q_e\varphi_0}{T_e}\right), \qquad (22)$$

$$\varepsilon_i = \frac{1}{2}m_i v^2 + q_i\varphi, \qquad \varepsilon_e = \frac{1}{2}m_e v^2 + q_e\varphi,$$

Here n_m is the density at mirror throat, q_i, q_e are ion, electron charge, respectively and we let $B=B_0$, $\varphi=\varphi_0$ at the mirror throat, and $B=B_b$, $\varphi=\varphi_b$ at the midplane. Hereafter in this section we drop subscripts i and e for simplicity. The passing particles exist in the region $\varepsilon \geqq \mu B + q\varphi$ and $\varepsilon \geqq \mu B_0 + q\varphi_0$ in Fig.1(b) and the passing particle density n_p is obtained by integration of Eq.(22) over the passing particle region as follows,

$$n_p = n_m \exp(-\delta\varphi)\left\{erfc\{(-\delta\varphi)^{1/2}\}\right.$$

$$\left. - \left(1 - \frac{1}{R}\right)^{1/2} \exp\left(-\frac{\delta\varphi}{R-1}\right) erfc\left\{\left(-\frac{R}{R-1}\delta\varphi\right)^{1/2}\right\}\right\}, \qquad \delta\varphi \leqq 0,$$

$$n_p = n_m \exp(-\delta\varphi)\left\{1 - \left(1 - \frac{1}{R}\right)^{1/2} \exp\left(-\frac{\delta\varphi}{R-1}\right)\right\}, \qquad \delta\varphi > 0. \qquad (23)$$

Here,

$$\delta\varphi = \frac{q(\varphi-\varphi_0)}{T}, \qquad R = B_0/B,$$

$$erfc\{x\} = 2\int_x^\infty \exp(-t^2)dt/\sqrt{\pi}.$$

Here we assume $R \geqq 1$. Though this code follows the passing particle distribution, we use Eq.(23) to calculate the potential profile in favor of the computer time and numerical accuracy.

This code does not follow the Yushimanov trapped particles because only the dynamics of the particles passing through the midplane are calculated as already stated below Eq.(10). Then we approximate the distribution function of Yushimanov trapped particles as the same as that of passing particles in Eq.(23). The density n_y of Yushimanov trapped particles is given by,

$$n_y = n_m\sqrt{(R-1)/R}\exp(-\frac{R}{R-1}\delta\varphi)\{1-erfc\{(\frac{R_b}{R_b-1}\delta\varphi_b-\frac{R}{R-1}\delta\varphi)^{1/2}\}\}$$

$$-n_m\sqrt{(R_b-R)/R}\exp\{\frac{R}{R_b-R}\delta\varphi-\frac{R_b}{R_b-R}\delta\varphi_b\}D_s\{(\frac{R}{R_b-R}(\delta\varphi_b-\delta\varphi)$$

$$-\frac{1}{R_b-1}\delta\varphi_b)^{1/2}\},$$

for the case that,

$$\frac{R_b}{R_b-1}\delta\varphi_b \geqq \frac{R}{R-1}\delta\varphi, \quad \frac{R}{R_b-R}(\delta\varphi_b-\delta\varphi) \geqq \frac{1}{R_b-1}\delta\varphi_b,$$

and $\delta\varphi \geqq 0$,

$$n_y = n_m \exp(-\delta\varphi)\,[1-erfc\{(-\delta f)^{1/2}\}]$$

$$+ n_m\sqrt{(R-1)/R}\exp\left(-\frac{R}{R-1}\delta\varphi\right)\left[erfc\left\{\left(-\frac{R}{R-1}\delta\varphi\right)^{1/2}\right\}\right.$$

$$\left.-erfc\left\{\left(\frac{R_b}{R_b-1}\delta\varphi_b-\frac{R}{R-1}\delta\varphi\right)^{1/2}\right\}\right]$$

$$- n_m\sqrt{(R_b-R)/R}\exp\left\{\frac{R}{R_b-R}\delta\varphi-\frac{R_b}{R_b-R}\delta\varphi_b\right\}D_s\left\{\left(\frac{R}{R_b-R}(\delta\varphi_b-\delta\varphi)\right.\right.$$

$$\left.\left.-\frac{1}{R_b-1}\delta\varphi_b\right)^{1/2}\right\}, \qquad (24)$$

for the case that,

$$\frac{R_b}{R_b-1}\delta\varphi_b \geqq \frac{R}{R-1}\delta\varphi, \quad \frac{R}{R_b-R}(\delta\varphi_b-\delta\varphi) \geqq \frac{1}{R_b-1}\delta\varphi_b,$$

and $\delta\varphi < 0$,

$n_y = 0$, *for other cases.*

Here,

$$D_s\{x\} = 2\int_0^x \exp(t^2)\,dt/\sqrt{\pi},$$

$$\delta\varphi_b = \frac{q(\varphi_b-\varphi_0)}{T}, \qquad R_b = B_0/B_b.$$

Here we assume $R \geqq 1$ and $R_b \geqq 1$. Then we determine the potential profile by solving charge neutrality equation $n_i(R,\varphi)=n_e(R,\varphi)$.

This scheme resembles to that of Ref. (12). If the population of mirror trapped ion is very small, we may have multi-valued solution of potential in the neighborhood of mirror throat. However in this electron heating problem we obtain the proper solution for the potential from the charge neutrality equation[12].

4. Simulation Results

We show the results of the simulation of second harmonic electron resonance heating in the thermal barrier region of GAMMA 10. Figure 2 shows the schematic diagram of GAMMA 10 magnetic field profile used in the simulation. The thermal barrier is to be created in the axi-symmetric plug/barrier region[3]. The microwave is localized around the midplane. We assume that to the left of the magnetic throat of the plug/barrier cell there fills a Maxwellian plasma with density $10^{12} cm^{-3}$ and temperature 100 eV standing for the central cell plasma. In the simulation we assume $N_\perp = 1$, $k_\parallel = 0$ at second harmonic resonance.

We assume the profile of $|E^+|$ as $|E^+(z)| = |E_0^+| \max(1-25(z-1/2)^2, 0)$. Here the system length of mirror cell is normalized to be unity, and midplane is at z = 1/2 in the simulation. In this electric field profile, the magnetic field of the point $|E^+(z)|^2 = |E_0^+|^2/2$ is $B(z) = 1.05B_b$. The electrons trapped magnetically in the region $|E^+(z)|^2 \geqq |E_0^+|^2/2$ are expected

to be mainly heated. Those electrons are localized in the region $|90^\circ - \theta| \leqq 12^\circ$ in the electron velocity space. Here θ is electron pitch angle. This is the reason of $\Delta\theta=12^\circ$ in Sec.2.

Figure 3(a) shows the bounce averaged Fokker-Planck diffusion coefficient for the case of $|\vec{E_0}|=100V/cm$ at the midplane. It is seen that the resonant RF diffusion is localized along the $v_{\parallel}=0$ line . Although this field strength should be externally determined, hot electron formation and losses are calculated consistently with the microwave power.

Figure 3(b) shows the amplitude of the diffusion coefficient along $v_{\parallel}=0$ line. This coefficient is proportional to energy E consistently with what is expected from Eq.(2). In the region $E \geqq 50keV$ this coefficient becomes small due to the relativistic electron mass shift.

First we show the hot electron build up before the collisional process of hot electron is dominant. Here we assume $n_e=10^{12}cm^{-3}$, $T_e=100eV$, $T_i=100eV$ and $\varphi=0$ at the mirror throat as a boundary condition. As a initial condition we assume there are Maxwell distribution functions of hydrogen ions and electrons at the midplane of which density and temperature are the same as that of mirror throat. Then $\varphi = 0$ everywhere along z at t = 0.

Figure 4 shows the time variations of the electrostatic potential φ, the total density n, the hot electron density n_h, and the hot electron mean energy T_h at the midplane for the case of $|\vec{E_0}|=500V/cm$. Here hot electrons are defined as the electrons with energy larger than 2 keV at the midplane. Hot electrons build up at

early time and quasi-steady state is realized. In this build up phase the hot electron or ion collisional effects are neglected compared with the RF diffusion. The electrostatic potential dip is formed at the midplane.

The velocity distribution of the electrons and ions at the midplane at 3.0μsec are plotted in Fig.5. It is seen that the electrons are heated by ECRH in the $v_\perp$ direction. The electron distribution function is streched strongly around $v_\parallel=0$ line so that its amplitude is smaller than that on the both sides. On the other hand ions are not heated at all but modified from Maxwellian due to the acceleration by the electrostatic potential difference between mirror throat and the midplane. The collisional effects do not play any roll for the hot electron build up in this early phase.

Figure 6 is the electron distribution on $v_\parallel=0$ line as a function of electron energy E at 3.0μsec corresponding to that in Fig.5. Electron distribution function is proportional to E^{-1} in the high energy region, from which Eq.(6) is justified. The distribution function becomes small in the region larger than 50keV.

Next we study the hot electron build up in longer time scale. We examine the results of $|E_0^*|=100V/cm$, because the RF diffusion phase and the later phase of the slow build up of hot electrons are clearly observed in one figure. Figure 7 shows the time evolutions of the electrostatic potential, the total density, the hot electron density and the hot electron mean energy at the midplane. In the early phase before 150μsec, a quick build-up is observed in the hot electron density and in its mean energy in the same way as seen in Fig.4.

However after 150μsec, in contrast to the mean energy, the hot electron density continues to increase with lower growth rate. The latter process proceeds in the time scale of $\sim 1msec$ associated with the pitch angle scattering of hot electrons. The mechanism of the slow build-up of hot electron population may be understood as the balance of diffusional feed of particles driven by RF along the characteristic line $v_{\parallel}=0$ and the collisional drain from the RF diffusion zone. The RF diffusion tends to establish a velocity distribution function as shown in Eq.(6) along $v_{\parallel}=0$ line in a few tens of μsec. A net particle flow appears along $v_{\parallel}=0$ line only when particles are removed from the diffusion zone, which flow represents the build-up rate of the hot electron density. Because the pitch angle scattering does not change the particle energy, the mean energy remains the same in this phase. Electrostatic potential becomes negative in the first build up phase because electrons flow into the mirror trapped region from the passing region by ECRH, while ions are not affected by ECRH directly. In the second build up phase, however, the electrostatic potential turns back in the positive direction. This means that the collisional filling rate of the ions is larger than that of hot electron density build up by ECRH. At 3msec the final steady state is realized in the simulation.

Figure 8 shows the axial profiles of the magnetic field, potential, total density, and hot electron density in the steady state. Hot electrons are localized around the midplane and there are about 41% hot electrons at the midplane. Electrostatic potential also has a sharp profile around the midplane. Remarkable feature is

that electrostatic potential is negative at the midplane compared with that at the mirror throat even though any ion pumping is not included in the simulation. However this potential dip of -34eV is not sufficient as the thermal barrier against the passing electrons coming from the mirror throat with mean energy of 100eV. Density has its maximum value at the midplane which shows there are many ions trapped in the potential well at the midplane.

Figure 9 is the contour plot of the electron distribution function at the midplane in the steady state. The hot electrons are localized around the $v_{\parallel}=0$ line, i.e. resonance line. We believe from this contour that the hot electrons escape to the passing particle region by the electron drag but not by the hot electron pitch angle scattering, i.e. hot electrons scattered into off resonance region lose its energy by the electron drag and then are scattered into the passing particle region. This is supported by the analytical estimation in Sec.2. That is, the hot electron drag time is shorter than that of hot electron pitch angle scattering time to the passing particle region because $(\Delta\theta)^2 \sim 1$ in τ_{cs} and τ_{hs} of Eq. (9) in this case.

Figure 10 is the steady state electron distribution function at the midplane on $v_{\parallel}=0$ line as a function of electron energy E. This distribution function is proportional to E^{-1} in the high energy region, representing the dominant effect of the RF diffusion which maintains the steady state distribution of Eq. (6) along the resonance line $v_{\parallel}=0$.

5. Summary and Discussion

We have found that the hot electron density builds up in two phases with different mechanisms. We have also examined the potential evolution during the hot electron build up. The mechanism of the hot electron build up is as follows. At first electrons in the resonance region are accelerated by ECRH until they acquire the maximum energy limited by resonance detuning due to the relativistic electron mass shift. This first build up ends when the runaway electrons reach its maximum energy limit. While these hot electrons accumulate, the electrostatic potential at the midplane, becomes negative. This is the result of charge neutrality condition which requires faster accumulation of ions so as to balance the magnetically trapped hot electron population.

In the second phase hot electron pitch angle scattering play an important role of the hot electron density build up. The pitch angle scattering drives the hot electrons out of the resonance region of velocity space. The vacancies thus produced in the resonance region are filled by the RF diffusion from the cold electrons in a time scale of the first phase. Then hot electron density grows furthermore. In this second phase ions are collisionally trapped in the potential well so that the ion density also builds up. In the parameters used in our simulations ion trapping rate is larger than that of the hot electron build up time. Then the electrostatic potential dip decays in the second phase.

The ratio of the hot electron density to the total electron density at the midplane in the steady state is not so large in our

simulation which is 41% as is already shown. This ratio does not increase so much for $|\tilde{E_0}|$ larger than 100V/cm. However the density ratio will be increased by including the fundamemtal electron resonance heating, because the characteristic resonance line extends in the θ=45° direction in electron velocity space in GAMMA 10. In the steady state we found that the potential is negative at the midplane even though any ion pumping is not included in the simulatiom. However this potential dip is too small for the thermal barrier. Therefore necessity appears for pumping of the ions trapped in the thermal barrier potential.

References

[1] D.E.Baldwin and B.G.Logan,
Phys. Rev. Lett. 43, 1318(1979).

[2] R.H.Cohen, I.B.Bernstein, J.J.Dorning, and G.Rowland,
Nucl. Fusion 20, 1421(1980).

[3] M.Inutake, K.Ishii, A.Itakura, I.Katanuma, T.Kawabe,
Y.Kiwamoto, A.Mase, S.Miyoshi, T.Saito, K.Sawada,
D.Tsubouchi, K.Yatsu, M.Aizawa, T.Kamimura, R.Itatani,
and Y.Yasaka,
Nucl. Fusion Suppl. 1, 545(1983).

[4] B.W.Stallard, Y.Matsuda, and W.M.Nevins,
Nucl. Fusion 23, 213(1983).

[5] M.E.Mauel,
Phys. Fluids 27, 2899(1984).

[6] L.D.Pearlstein, T.B.Kaiser, and W.A.Newcomb,
Phys. Fluids 24 1326(1981).

[7] E.Otto, B.Hui, and K.R.Chu,
Phys. Fluids 23, 1031(1980).

[8] C.F.Kennel and F.Engelmann,
Phys. Fluids 9, 2377(1966).

[9] K.D.Marx,
Solution of a spatially dependent Fokker-Planck equation
for mirror confined plasma,
Ph.D Thesis, Univ. California (1968).

[10] J. Killeen and K.D. Marx,
Methods in Computational Physics, vol.9, p421,

(edited by E. Alder, Academic Press, New York).

[11] T.A. Cutler, L.D. Pearlstein, and M.E. Rensink,
Lawrence Livermore Laboratory, Rept. UCRL-52233 (1977).

[12] R.H.Cohen,
Nucl. Fusion 21, 209(1981).

Figure Captions

Fig.1(a)

Schematic diagram of single mirror and electrostatic potential profile. Here q is the charge of a particle.

Fig.1(b)

Particle velocity space diagram. ε and $\mu=mv_{\perp}^2/2B$ are the particle energy and the magnetic moment, respectively. B, φ are magnetic field and electrostatic potential, respectively. Subscripts 0 and b represent the quantities at the mirror throat and at the midplane, respectively.

Fig.2(a)

GAMMA 10 magnetic field profile along magnetic field line.

Fig.2(b)

Magnetic field profile used in the simulation. This profile is the same as that of plug/barrier region of GAMMA 10.

Fig.3(a)

Three dimensional plot of the bounce averaged Fokker-Planck diffusion coefficient C_{vv}. Here $C_{vv}=\int_{orbit} A_a dz/v_{\parallel} \; / \int_{orbit} dz/v_{\parallel}$ in Eq.(14). The Fokker-Planck collision term is omitted in this figure.

Fig.3(b)

Amplitude of C_{vv} along $v_{\parallel}=0$ line in Fig.3(a).

Fig.4

Time evolution of (a) the electrostatic potential, (b) the total density, (c) hot electron density, and (d) the hot electron mean energy, respectively at the midplane for the case of

$|\vec{E_0}|$ =500V/cm.

Fig.5

The contour plot of (a) electron and (b) ion distribution function at the midplane at t = 3.0 μsec for the case of $|\vec{E_0}|$ =500V/cm. Here $m_e v_{e0}^2/2 = 1keV$ and $m_i v_{i0}^2/2 = 1keV$.

Fig.6

The electron distribution function along $v_{\parallel}$=0 line at the midplane at 3.0 μsec for the case of $|\vec{E_0}|$ =500V/cm.

Fig.7

Time evolution of (a) the electrostatic potential, (b) the total density, (c) the hot electron density, (d) the hot electron mean energy, respectively at the midplane for the case of $|\vec{E_0}|$ =100V/cm.

Fig.8

(a) the magnetic field, (b) the electrostatic potential, (c) the total density, (d) the hot electron density profile along z in the steady state, respectively for the case of $|\vec{E_0}|$ =100V/cm.

Fig.9

The contour plot of the electron distribution function at the midplane in the steady state for the case of $|\vec{E_0}|$ =100V/cm. Here $ln(f_e)$ is plotted.

Fig.10

The electron distribution function along $v_{\parallel}$=0 line at the midplane in the steady state for the case of $|\vec{E_0}|$ =100V/cm.

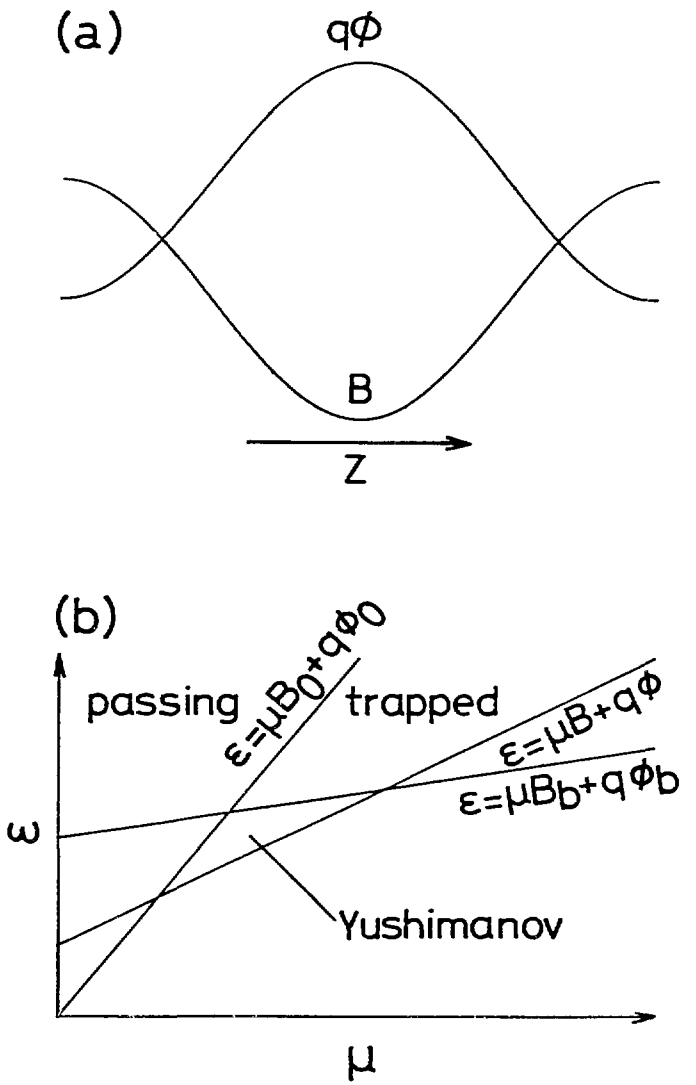
(a)
qφ
B
Z
(b)
passing
trapped
ε=μB0+qφ0
ε=μB+qφ
ε=μBb+qφb
Yushimanov
ω
μ

Fig. 1

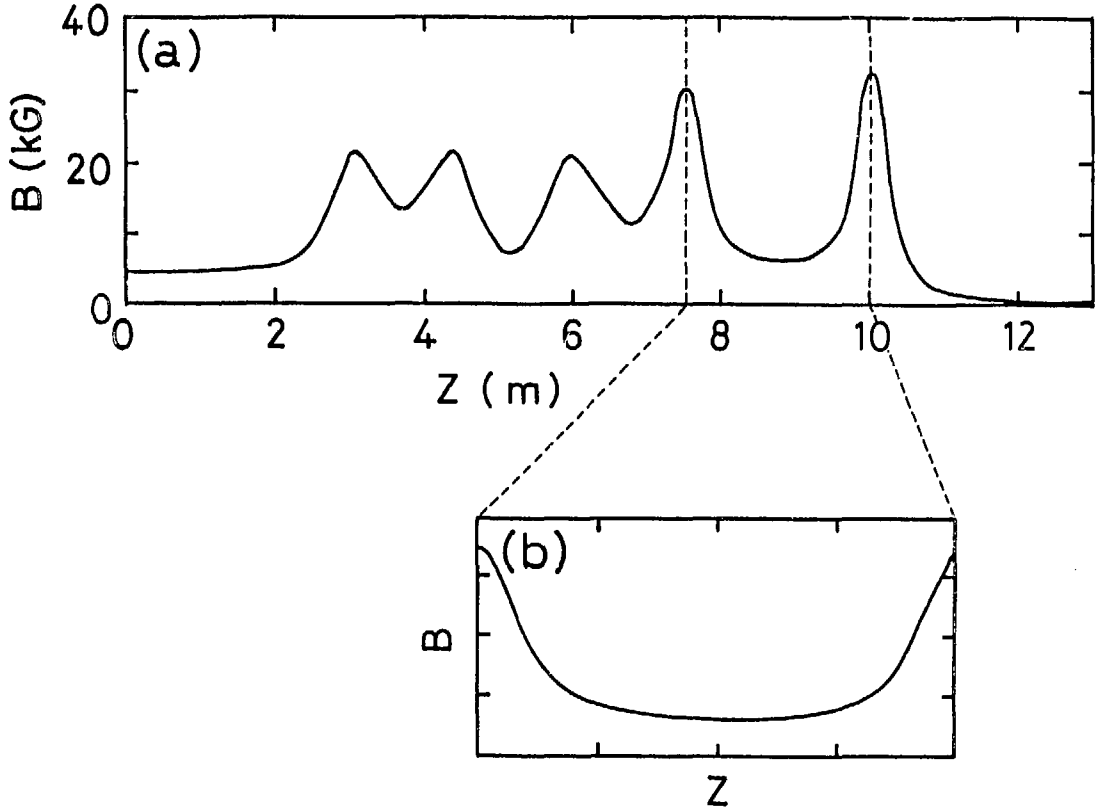

Fig. 2

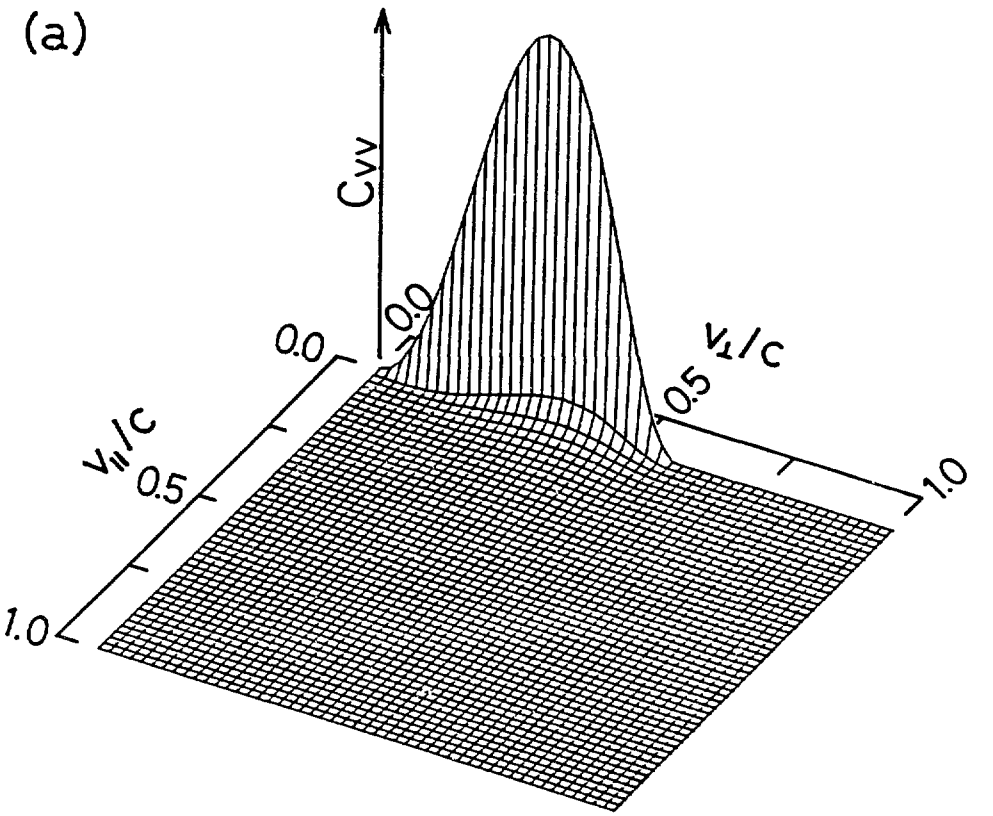

Fig. 3(a)

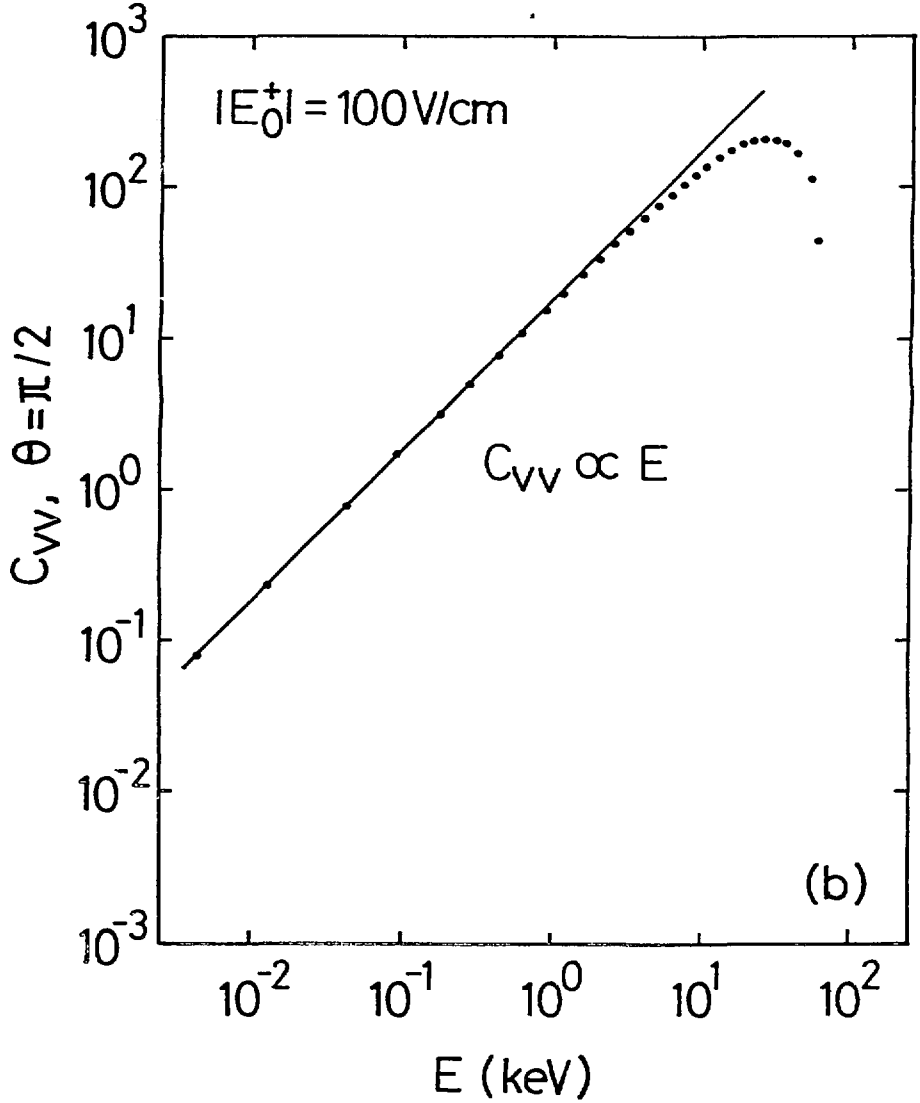
10^3
10^2
10^1
10^0
10^{-1}
10^{-2}
10^{-3}
$|E_0^+| = 100$ V/cm
$C_{VV} \propto E$
(b)
C_{VV}, $\theta = \pi/2$
10^{-2}
10^{-1}
10^0
10^1
10^2
E (keV)

Fig. 3(b)

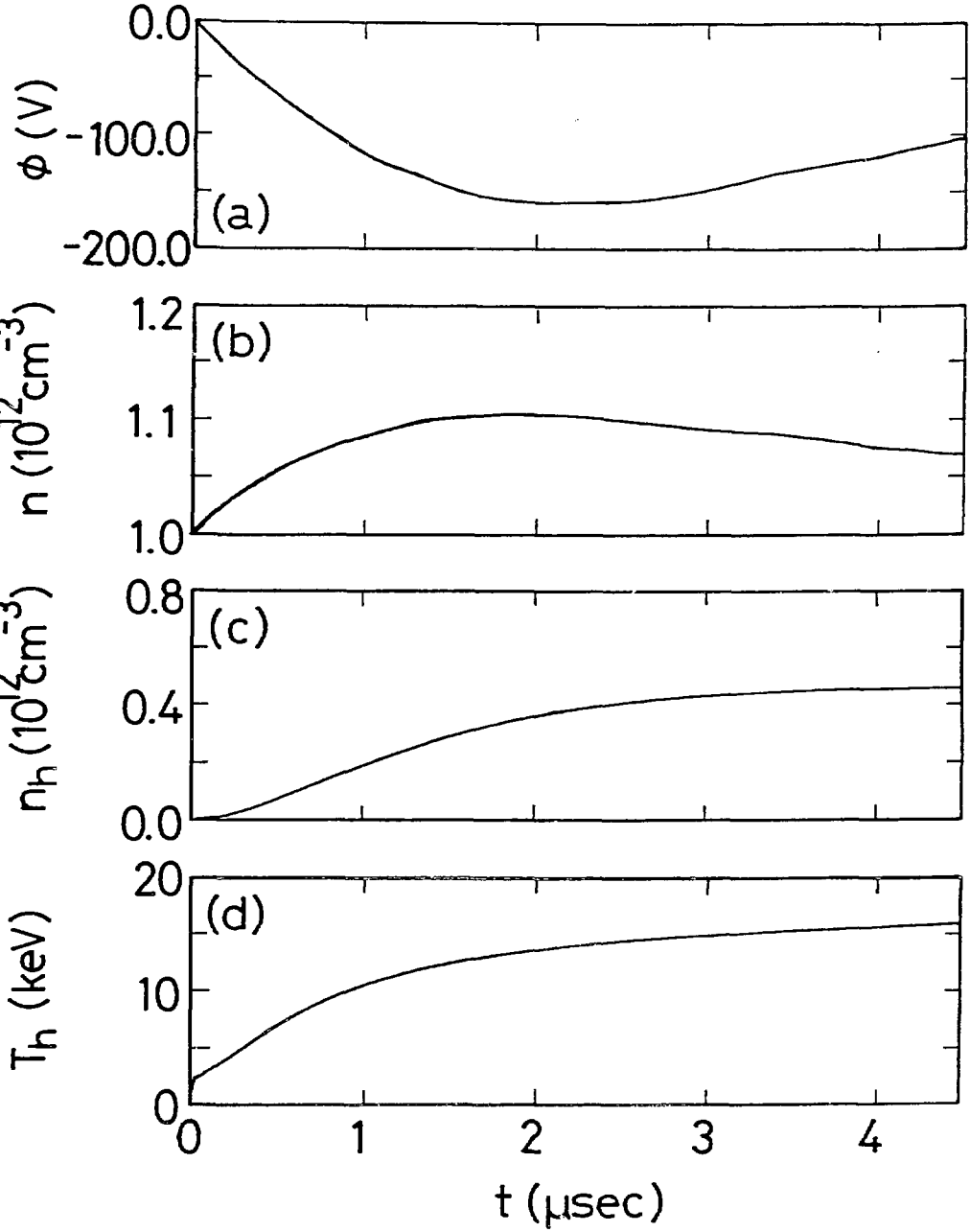
0.0
-100.0
-200.0
φ (V)
(a)
1.2
1.1
1.0
n (10^12cm^-3)
(b)
0.8
0.4
0.0
n_h (10^12cm^-3)
(c)
20
10
0
T_h (keV)
(d)
0
1
2
3
4
t (μsec)

Fig. 4

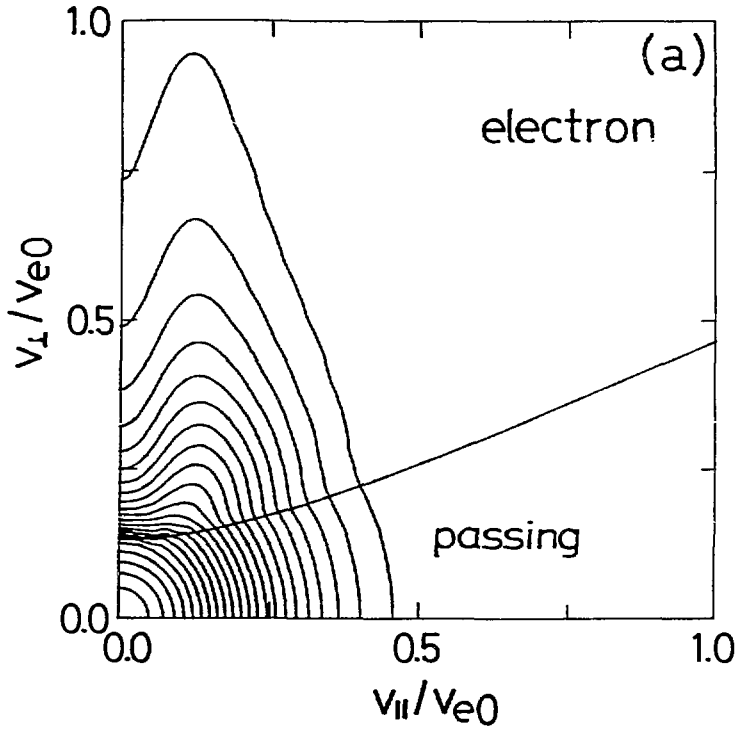
(a)
electron
passing
1.0
0.5
0.0
0.0
0.5
1.0
$v_\perp / v_{e0}$
$v_\parallel / v_{e0}$

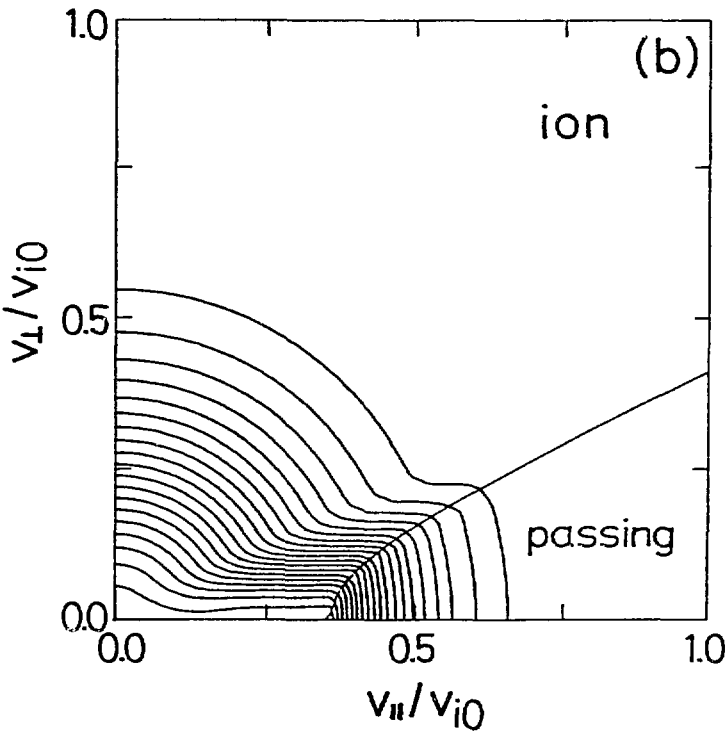
(b)
ion
passing
1.0
0.5
0.0
0.0
0.5
1.0
$v_\perp / v_{i0}$
$v_\parallel / v_{i0}$

Fig. 5

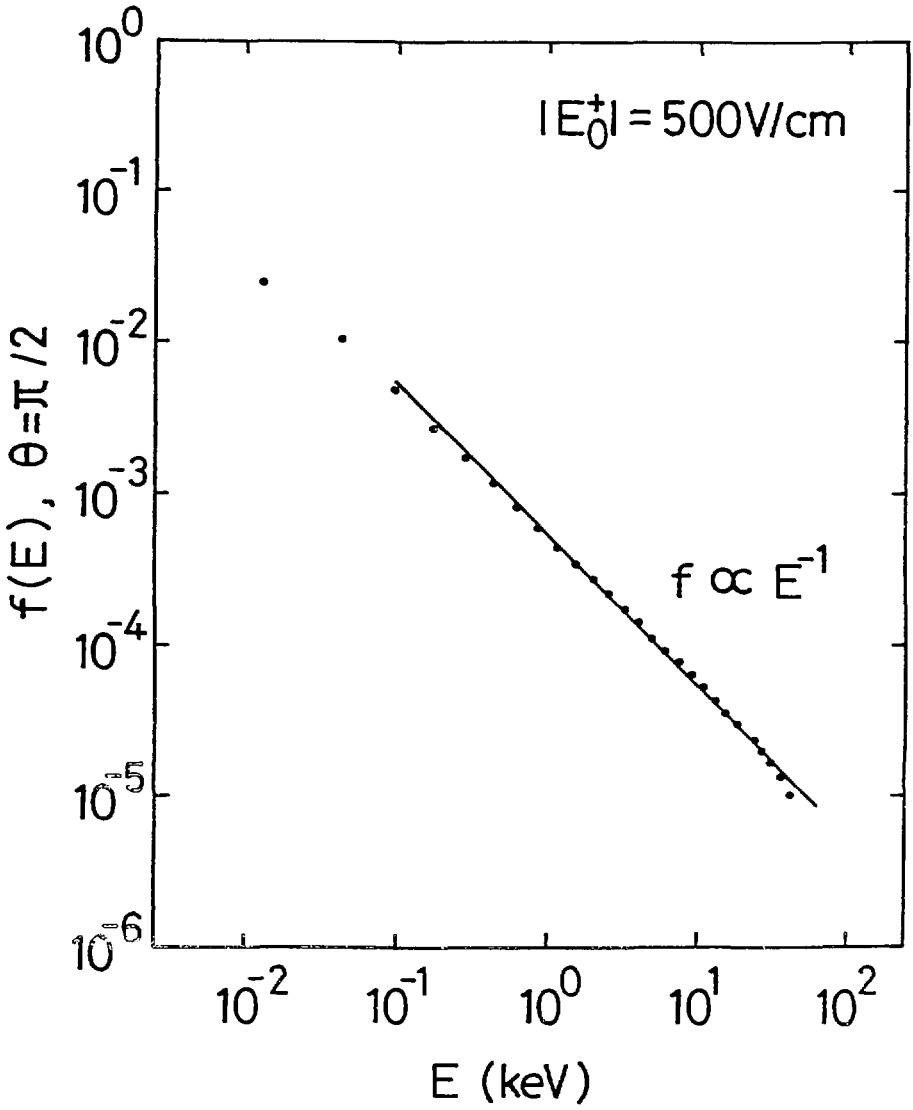
10^0
10^{-1}
10^{-2}
10^{-3}
10^{-4}
10^{-5}
10^{-6}
f(E), θ=π/2
$|E_0^+| = 500V/cm$
$f \propto E^{-1}$
10^{-2}
10^{-1}
10^0
10^1
10^2
E (keV)

Fig. 6

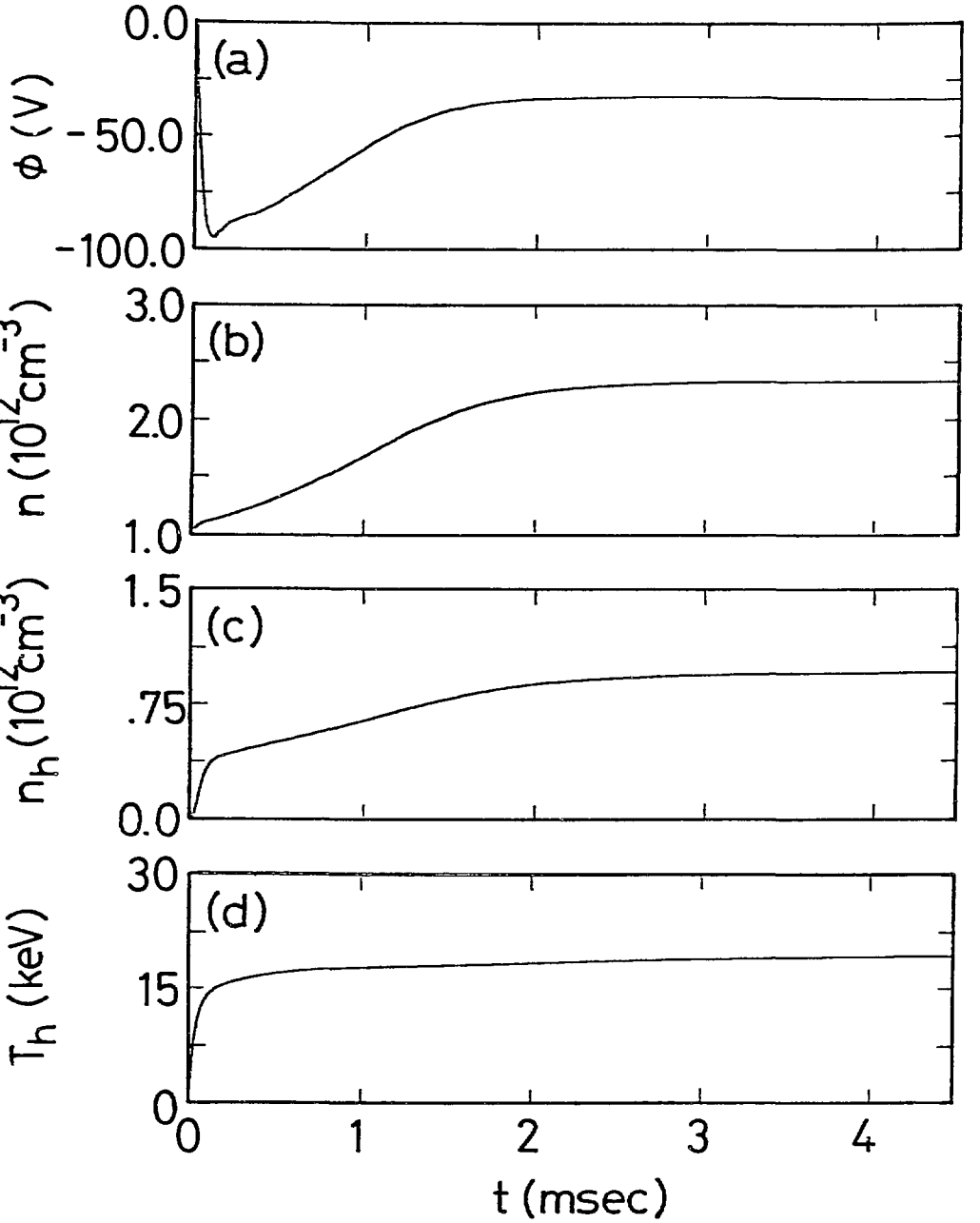
0.0
(a)
φ (V)
-50.0
-100.0
3.0
(b)
n (10^12 cm^-3)
2.0
1.0
1.5
(c)
n_h (10^12 cm^-3)
.75
0.0
30
(d)
T_h (keV)
15
0
0
1
2
3
4
t (msec)

Fig. 7

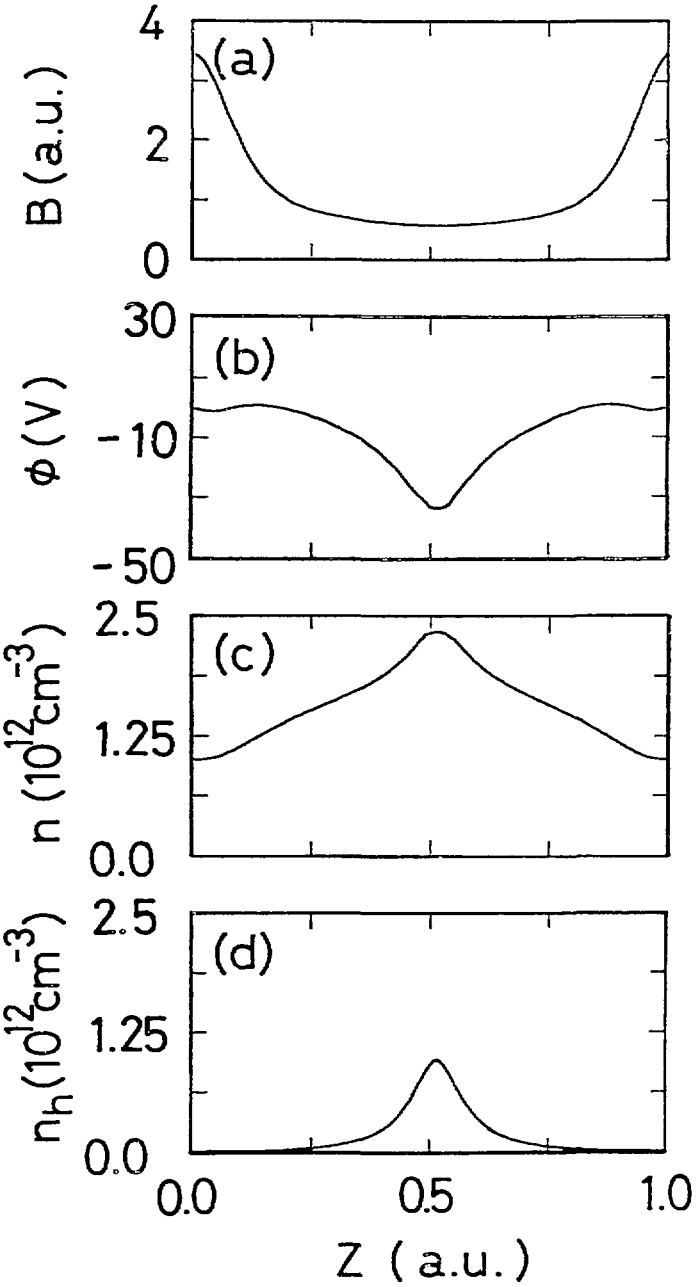
4
2
0
B (a.u.)
(a)
30
-10
-50
φ (V)
(b)
2.5
1.25
0.0
n (10^{12}cm^{-3})
(c)
2.5
1.25
0.0
n_h (10^{12}cm^{-3})
(d)
0.0
0.5
1.0
Z (a.u.)

Fig. 8

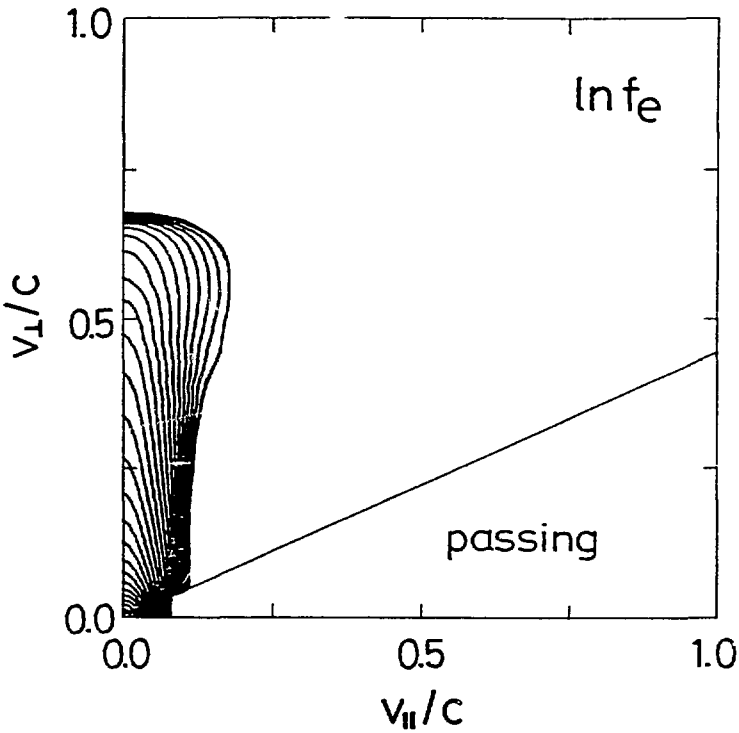

Fig. 9

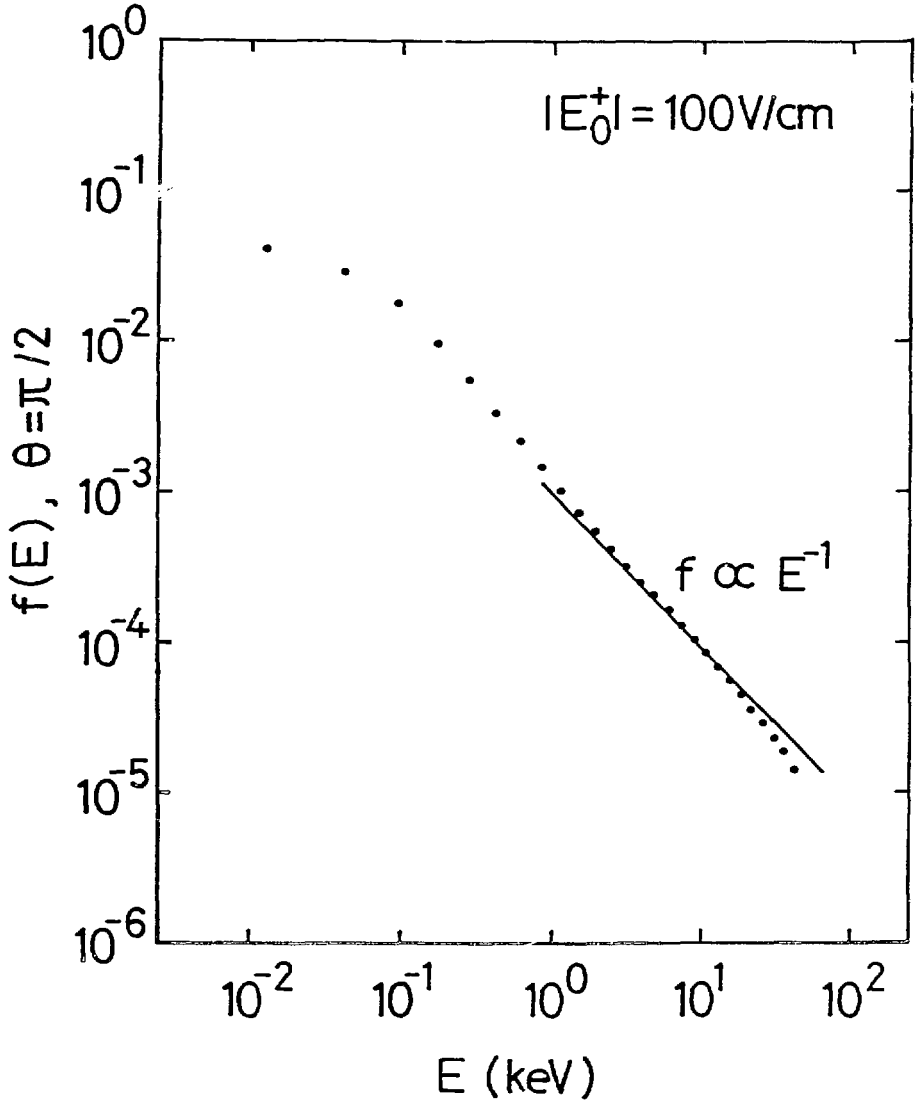
10^0
10^{-1}
10^{-2}
10^{-3}
10^{-4}
10^{-5}
10^{-6}
$|E_0^+| = 100 V/cm$
$f \propto E^{-1}$
f(E), θ=π/2
10^{-2}
10^{-1}
10^0
10^1
10^2
E (keV)

Fig. 10